J Therm Anal Calorim (2016) 125:1205–1215
DOI 10.1007/s10973-016-5586-4

Chromium-modified zinc oxides

Wojciech Gac[1] · Witold Zawadzki[1] · Grzegorz Słowik[1] · Magdalena Greluk[1] · Justyna Pawlonka[1] · Andrzej Machocki[1]

Received: 10 November 2015 / Accepted: 21 May 2016 / Published online: 18 June 2016

Abstract Zinc oxides modified with chromium were prepared by the co-precipitation method. Samples were calcined at 400 °C. Structural and surface properties of materials were studied by means of transmission electron microscopy, X-ray diffraction and low-temperature nitrogen adsorption methods. Temperature-programmed reduction methods were used for investigation of the influence of chromium on the redox properties of zinc oxides. The nature of surface sites and the course of surface reactions occurred during methanol decomposition were determined by the temperature-programmed desorption of methanol with detection of evolved gasses by mass spectrometry and in situ diffuse reflectance infrared Fourier transform spectroscopy. We have found that modification of ZnO with chromium led to the increase of the specific surface area of oxides and decrease of mean crystallite size of ZnO. Partial incorporation of chromium ions to the hexagonal ZnO structure, formation of strongly dispersed spinel ($ZnCr_2O_4$) and chromium zinc oxide species ($ZnO{\cdot}CrO_3$) was observed. We have stated that methanol was adsorbed on the surface of ZnO at 100 °C mainly via formation of methoxy species, and the main products of methanol desorption were carbon monoxide and hydrogen. The presence of chromium facilitated direct oxidation of methoxy groups to formate species at low temperatures ($\sim$100 °C) and their transformation to hydrogen and carbon dioxide during temperature-programmed desorption. The enhanced transformation of methoxy to formate species was attributed to the labile oxygen in chromium-modified zinc oxides.

Keywords Zinc oxide · Chromium · Methanol desorption · TPR · TPD · DRIFTS

Introduction

Zinc oxide has been widely used in rubber industry, production of ceramics, concrete, cosmetics and personal care, surface coatings, pharmaceuticals and foods [1]. An increase of the interests of application of ZnO in the emerging technologies is observed [2, 3]. Zinc oxide has been proposed for the production of light-emitting and laser diodes [4, 5], varistors [6], sensors [7, 8], magnetic materials [9] and photocatalysts [10]. This oxide has been used as an adsorbent for purification of gas streams and component of industrial catalysts, mainly for hydrogenation and dehydrogenation reactions. Pure zinc oxide shows relatively low thermal stability. The increase of the specific surface area and retardation of sintering of ZnO particles have been often achieved by the introduction of additional metal oxides. Modification of ZnO, especially for rubber production, has been often reached by functionalization of the surface of ZnO particles with silica, alumina, siloxane groups, deposition of organic and polymeric protecting layers [11]. In 1923, BASF introduced zinc oxide/chromium oxide catalysts for high-pressure methanol synthesis [12]. The catalysts were obtained by mixing of chromic acid with an aqueous suspension of zinc hydroxide or in simpler way, by mixing of zinc oxide powder with chromic oxide. In the next years, the catalysts based on the mixtures of oxides or made by co-precipitation of soluble zinc and chromium salts were developed and offered by BASF, Du

✉ Wojciech Gac
wojciech.gac@umcs.lublin.pl

[1] Department of Chemical Technology, Faculty of Chemistry, Maria Curie-Sklodowska University, 3 M. Curie-Sklodowska Sq., 20-031 Lublin, Poland

Pont, Montedison, ICI [12]. High activity in methanol synthesis has been observed for Cu/ZnO catalysts since 1930s of the last century. However, such catalysts suffered from rapid deactivation due to sintering. The breakthrough in methanol synthesis (resulted further in the development of low-pressure methanol plants) was done in the 1960s by modification of Cu/ZnO catalysts with promoters, such as the oxides of Al, Cr or Mn. Similar CuO/ZnO catalysts, modified with alumina or chromium oxide, were used for water gas shift reaction (WGS) in ammonia synthesis plants. The beneficial properties of such catalysts were mainly ascribed to the presence of zinc aluminate or chromite spinels, which improved stability of zinc oxide. In spite of large efforts and a reach literature, further studies are necessary to better understand the nature of catalytic active sites and develop new catalysts.

The improvement of zinc oxide-based catalysts is today of vital importance. Zinc oxide has been recently proposed for numerous reactions, including desulfurization, transesterification of vegetable oils and fine chemical synthesis [13, 14]. Besides methanol synthesis and water gas shift reaction, two additional processes become today of prime interests, i.e. carbon dioxide conversion with hydrogen to methanol and steam reforming of methanol [15, 16]. Carbon dioxide is produced worldwide via combustion of fossil fuels. The increase of global temperature is perceived as result of increase of CO_2 concentration in atmosphere from 300 ppm on the pre-industrial level to nearly 400 ppm. Synthesis of methanol from CO_2, which could be captured from the fossil fuel combustion processes, and hydrogen obtained by the use of renewable energy is regarded as one of the most promising ways of carbon capture and utilization technologies [17]. Methanol is produced today in the large scale by conversion of carbon monoxide with hydrogen adding small amounts of carbon dioxide, mainly in the presence of modified copper zinc oxide catalysts. New catalysts for direct conversion of carbon dioxide with hydrogen to methanol can be obtained by the application of new improved supports, such as chromium-modified zinc oxides, and hence, better understanding of surface phenomena is indispensable. In turn, hydrogen can be produced *on-site* in the small stationary or portable systems by the steam reforming of methanol. The main reaction products of this reaction are hydrogen and carbon dioxide. Such mixture after removal of the traces of carbon monoxide can be used in the low-temperature proton exchange membrane fuel cells (PEMFC) or even directly in the Internal Reforming Methanol Fuel Cell (IRMFC) for electricity production [18]. Better insight into the properties of chromium-modified zinc oxide supports may bring progress in the development of new catalysts for the steam reforming of methanol. Such catalysts should show high activity, low selectivity to carbon monoxide, high durability and thermal stability in transient conditions.

The aim of the studies was the synthesis of novel chromium-modified zinc oxide materials, elucidation of the role of chromium on the structural, surface and redox properties of the samples and determination of the course of surface reactions during methanol desorption with regard to the potential application of such oxide materials as the supports and/or catalysts for CO_2 hydrogenation and steam reforming of methanol.

Experimental

Sample preparation

Zinc oxide was prepared by the precipitation method. Zinc acetate ($Zn(CH_3COO)_2{\cdot}2H_2O$) was dissolved in distilled water and precipitated with aqueous solution of ammonium carbonate ($(NH_4)_2CO_3$). The precipitating agent was slowly introduced with the constant rate to pH = 8.5. The mixture was then filtered under vacuum and flushed with water and ethanol. The sample was dried at 120 °C and calcined at 400 °C for 6 h. Chromium-modified zinc oxides (denoted as ZnO–Cr–x) were obtained by the co-precipitation method. Suitable amounts of zinc acetate ($Zn(CH_3COO)_2{\cdot}2H_2O$) and chromium nitrate ($Cr(NO_3)_3{\cdot}9H_2O$) were dissolved in distilled water and then co-precipitated with aqueous solution of ammonium carbonate in the same conditions as above. Next similar procedures of filtering, drying and calcination as in the synthesis of unmodified ZnO were applied.

Experimental techniques

X-ray diffraction studies (XRD) were done with Empyrean (PANalytical) diffractometer using Cu–K_α radiation ($\lambda = 1.5418$ Å). A standard procedure of profile fitting analysis was performed using HighScore Plus program, which included: background determination, peak searching, profile fitting and overlapping peaks deconvolution, K-alpha2 peaks removing and determination of width at half maximum (FWHM) of selected deconvoluted peaks. Mean size of ZnO crystallites (d_x) was calculated from the broadening of the deconvoluted ZnO XRD peaks using the Warren–Scherrer equation [19]:

$$d_x = \frac{0.9\lambda}{(B_1^2 - B_2^2)^{1/2}\cos\theta}$$

where θ, diffraction angle; λ, X-ray wavelength (1.54179 Å for Cu lamp); B_1, peak width at half maximum (FWHM) of the reflection; and B_2, peak width of the

standard. The discussion was based on the results for ZnO (110) peak due to its high intensity and relatively small effects of other phases.

The nitrogen adsorption/desorption isotherms were obtained volumetrically at −196 °C using ASAP 2405N analyzer (Micromeritics Instrument Corp.). Samples were outgassed under low pressure ($\sim 10^{-2}$ Pa) at 200 °C. The adsorption data were used to evaluate the specific surface area (S_{BET}). The total pore volume (V_p) was determined on the basis of nitrogen amount adsorbed at relative pressure of about $p/p^\circ = 0.98$. Keeping in mind some limitation of different models, the structural data were estimated from the adsorption branch of isotherms by applying the Barrett–Joyner–Halenda (BJH) method [20].

The samples for microscopic studies were grinded in an agate mortar to a fine powder. The resulting powder was poured with absolute ethanol to form a slurry. The sample was inserted into the ultrasonic homogenizer for 20 s. Then, the slurry was introduced to a copper grid covered with formvar stabilized with carbon. The sample was left on the filter paper until ethanol was evaporated. The transmission electron microscope Titan G2 60–300 kV FEI Company with an accelerating voltage of the electron beam equal to 300 kV was used in the studies of the samples by the scanning transmission electron microscopy–energy-dispersive X-ray spectroscopy technique (STEM-EDX). The transmission electron microscopic studies (TEM) of the samples were carried out with TEM microscope Tecnai G20 X-TWIN FEI Company using an accelerating voltage of the electron beam equal to 200 kV.

Redox properties of materials were investigated by the temperature-programmed reduction (TPR) and reduction/oxidation methods (TPR/TPO/TPR). Studies were carried out in the TPR apparatus Autochem 2920 (Micromeritics Instrument Corp.). Samples ($m = 0.05$ g) in the TPR studies were initially heated in the flow of helium up to 150 °C and after 30 min of isothermal treatment were cooled down to −70 °C. The reduction was performed in the flow of the mixture 5 vol% H_2 in Ar ($Q = 30$ cm^3 min^{-1}) up to 600 °C with linear ramp rate 10 °C min^{-1}. The evolved water was removed from the stream of carrier gas in a cold trap with the LN_2–isopropanol mixture at −77 °C, maintained between reactor and thermal conductivity detector (TCD). Samples in the TPR/TPO/TPR experiments after similar pre-treatment procedure as in TPR studies were reduced with linear ramp rate 10 °C min^{-1} from −70 to 350 °C and then at 350 °C for 1 h (TPR-1). The samples were next cooled down to −70 °C in the flow of He. The inert gas was then switched for the mixture 5 vol% of O_2 in He ($Q = 30$ cm^3 min^{-1}), and the samples were oxidized under the linear ramp rate 10 °C min^{-1} up to 100 °C. The oxidizing mixture after 1 h was changed to He, and the temperature was decreased to −70 °C. Next the reduction–oxidation procedures were repeated, while oxidation temperature was successively increased to 200, 300 °C and finally to 400 °C.

Methanol temperature-programmed desorption studies (TPD-MS) were carried out in the reaction system coupled with mass spectrometer HAL201RC (Hiden Analytical). The samples were initially heated in the flow of He up to 350 °C and then after 1 h were cooled down to 100 °C. Methanol was adsorbed at 100 °C from the He stream, which was passed through methanol saturator maintained at 15 °C. The samples, after flushing with He, were heated with 10 °C min^{-1} ramp rare. The MS intensities of selected ions were recorded. The nature of the species formed on the surface of oxides during methanol temperature-programmed desorption was studied by diffuse reflectance infrared Fourier transform spectroscopy (DRIFTS). The samples were subjected to the same procedures as in the TPD-MS studies, using Ar as carrier gas. FTIR spectrometer (Nicolet 6700, Thermo Scientific) was equipped with LN_2 cooled MCT/A detector. Samples were introduced into the Praying Mantis High-Temperature Reaction Chamber (Harrick), which was covered by a dome with ZnSe windows. DRIFTS spectra were collected during Ar pre-treatment, methanol adsorption and desorption at selected temperatures with the resolution of 4 cm^{-1} and maximum source aperture. Interferograms of 256 scans were averaged for each spectrum. The spectra were corrected by applying the background signal recorded for KBr powder.

Results and discussion

Phase composition

The content of chromium in modified zinc oxides was varied from 3.33 to 17.1 mass% (Table 1). The results of X-ray diffraction studies of the samples are presented in Fig. 1. ZnO hexagonal structure with the space group $C_{6v}^4 - P6_3mc$ (ICDD: ZnO-04-008-8199) is observed in the unmodified and chromium-modified oxide materials. The mean crystallite size decreases from 23 nm in ZnO sample to 5.1 nm in ZnO–Cr-3 sample (Table 1). Gradual broadening of ZnO peaks with the increase of chromium content indicates the decrease of the size of ZnO particles. The diffraction peaks of zinc oxide in ZnO–Cr–x samples are located at slightly higher diffraction angles than pure ZnO. Gradual shift is observed with an increase of chromium content (Table 1). Such changes could result from the reduction in lattice constant and decrease of the volume of the unit cell. The lattice contraction could be ascribed to the variation of the surface stresses, due to the crystallite size decrease [21]. Other possible explanation is partial

Table 1 Specific surface area (S_{BET}), total pore volume (V_p), mean pore diameter (D_p) of the samples, mean crystallite size (d_x) of ZnO and position of XRD (110) reflection lines of ZnO

Sample	Cr content/wt%	$S_{BET}/m^2\ g^{-1}$	$V_p/cm^3\ g^{-1}$	D_p/nm	d_x/nm	XRD (110) (2θ)
ZnO	–	35.7	0.41	41.5	23.0	56.52
ZnO–Cr-1	3.33 ± 0.15	45.2	0.21	16.2	17.3	56.53
ZnO–Cr-2	13.00 ± 0.50	94.6	0.35	14.7	6.3	56.61
ZnO–Cr-3	17.10 ± 0.50	73.1	0.16	10.0	5.1	56.82

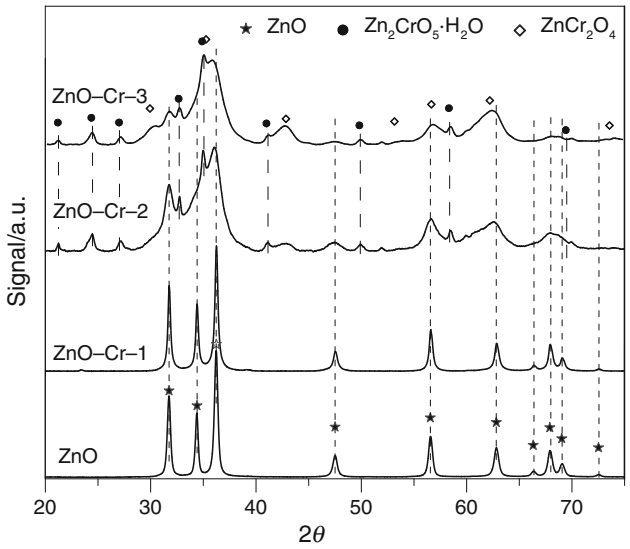

Fig. 1 XRD patterns of the samples

substitution of zinc ions in ZnO structure by smaller chromium ions. The effective ionic radius of Zn^{2+} is 0.74 Å, while the radius of Cr^{3+} equals 0.61 Å [22]. This may facilitate formation of point defects in ZnO structure, generation of Zn^{2+} vacancies and non-stoichiometry and hence alter the surface and catalytic properties of the materials used as the supports or catalysts.

XRD diffraction studies reveal the presence of dispersed zinc chromium oxide species. It is hard to unambiguously ascribe the peaks to the singular phase. The XRD peaks can be assigned to different oxide materials of Zn^{2+}, Cr^{3+} or Cr^{6+}, including spinel $ZnCr_2O_4$ (ICDD: $ZnCr_2O_4$-01-079-5291) and zinc chromium oxide phases of similar positions of reflection lines, including $4ZnO{\cdot}CrO_3{\bullet}3H_2O$ (ICDD: 00-011-0275), $2ZnO{\cdot}CrO_3{\bullet}H_2O$ (ICDD: 00-011-0276) or Zn_2CrO_5 (ICDD: 00-011-0277). Precipitation of zinc and chromium compounds with ammonium carbonate can initially drive to the formation of layered double hydroxides (LDHs) with hydrotalcite-like (HT) structure [23–25]. LDHs of general formulae $\left[M^{2+}_{1-x}M^{3+}_{x}(OH)_2\right]^{x+}\left[A^{n-}_{x/n}\right]\cdot mH_2O$ are composed of the divalent metal ions (M^{2+}) distributed within the layers containing trivalent metal ions (M^{3+}), separated by the layers of A^{n-} anions with negative charge n [23–25]. The value of x is related to the molar ratio of $M^{2+}/(M^{2+} + M^{2+})$ and generally is in the range 0.2–0.33. The intercalated anions maintain charge balance resulted from partial substitution of divalent by trivalent cations. Thermal treatment of hydrotalcite phases up to 200 °C leads initially to the dehydration of surface water and removal of crystallization water from interlayer regions [25]. The increase of treatment temperature up to 400 °C results in dehydroxylation and the loss of carbonate anions from the interlayer regions, which induce further structural changes of materials. Although HT structure can be retained in some oxide materials after calcination at 400 °C or recovered in contact with water and carbon dioxide, e.g. in LDHs containing Mg^{2+} or Al^{3+}, we have not observed such phases in the obtained ZnO–Cr samples. The presence of $ZnO{\cdot}CrO_3$ oxide phases results from oxidation of Cr^{3+} ions in calcination stage. The changes of the oxidation state of chromium ions during thermal treatment in air were reported in the literature for different hydrotalcite materials containing chromium [24–27]. Rives pointed out that Cr^{3+} in ZnCr hydotalcite materials can be oxidized to CrO_4^- below 400 °C with formation of amorphous zinc hydroxychromates, while thermal treatment of materials at higher temperatures may lead to the decrease of oxidation state of Cr^{6+} and formation of $ZnCr_2O_4$ spinel [26]. Similar changes of chromium oxides at high temperature are discussed in Ref. [28]. CrO_3 can be decomposed in air at elevated temperatures to the oxides of lower oxidation state, e.g. at 300 °C to Cr_6O_{15}, 420 °C to Cr_5O_9 and at 450 °C to Cr_2O_3 [28]. ZnO support may stabilize chromium oxides on the lower oxidation state of chromium and participate in the formation of $ZnCr_2O_4$ spinel phases. Zn^{2+} ions in spinels, especially in $ZnCr_2O_4$ non-stoichiometric spinel, can be located both in tetrahedral and in octahedral environment [28]. Erranni pointed out that the presence of surface octahedral zinc ions, i.e. located in the non-stoichiometric spinels, is crucial for high activity of catalysts in methanol synthesis [29]. He suggested that such sites are responsible for heterolytic dissociative adsorption of hydrogen.

Structural changes

The morphology and spatial distribution of elements in the samples obtained by STEM-EDX technique are presented in Fig. 2. STEM-EDX images of ZnO sample (Fig. 2a) show the assemblies of ZnO nanoparticles with elongated shape and uniform distribution of zinc and oxygen. An introduction of chromium induces structural changes and formation of much smaller nanoparticles. The nanoparticles in ZnO–Cr-1 are less regular than in the ZnO sample (Fig. 2b). An increase of chromium content leads to the increase of the amounts of amorphous-like phases. One can find irregular and rod-like agglomerates, composed of very small particles (Fig. 2c, d). Regular nanoparticles of ZnO are well visible on the TEM image (Fig. 3a). HRTEM image (see inset in Fig. 3a) reveals hexagonal arrangement of atoms in selected nanoparticle attached to the second one with different orientation. Particles of different size are well visible in the TEM image of ZnO–Cr-1 sample (Fig. 3b). ZnO–Cr-2 and ZnO–Cr-3 samples are composed of very small nanoparticles of different shape and orientation, which resemble amorphous-like phases observed in the STEM-EDX studies. The size of nanoparticles is below 10 nm. The results are similar to that obtained from XRD studies.

The specific surface area (S_{BET}) of the ZnO sample is 35.7 $m^2\ g^{-1}$ (Table 1). An introduction of chromium led to the increase of the specific surface area and to the changes of porosity of materials (Table 1). The shape of nitrogen isotherms of the samples is in general similar (Fig. 4), and close to that of II-type, according to the IUPAC recommendations [30]. The shape of hysteresis loop for ZnO sample is close to H3 type and indicates the presence of slit-shaped pores. Such pores may result from the spatial arrangement of nanoparticles of uniform planes and close attachment of elongated agglomerates, well visible on the TEM images (Fig. 3a). In the case of chromium-modified oxides, the hysteresis loops are wider and are shifted to lower values of relative pressures, indicating different pore size distribution. Total pore volume (V_p) and mean pore diameter (D_p) of the ZnO sample are equal to 0.41 $cm^3\ g^{-1}$ and 41.5 nm, respectively. The decrease of total pore volume and mean pore diameter is observed with an increase of chromium content. High surface area or low crystallite size of the oxides could be obtained under optimal Cr/Zn ratio and calcination temperature [31, 32].

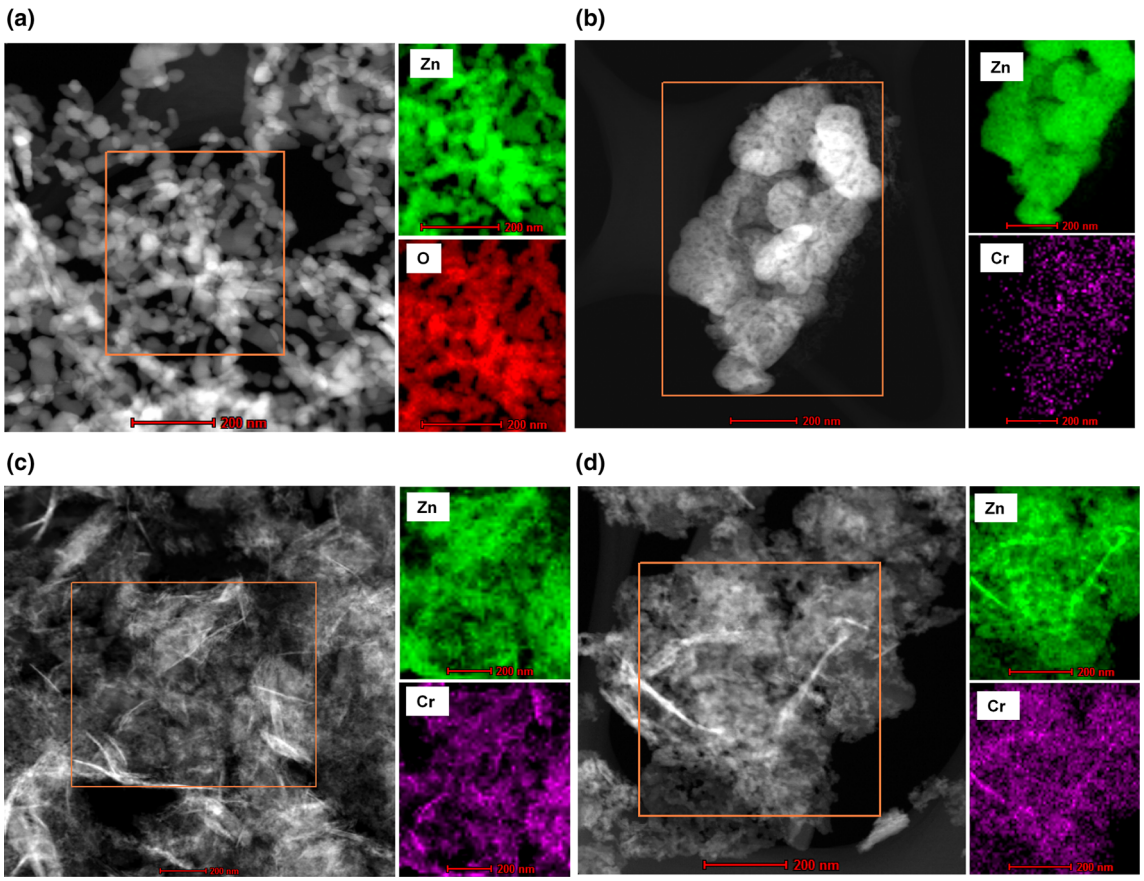

Fig. 2 STEM-EDX images of the samples: **a** ZnO, **b** ZnO–Cr-1, **c** ZnO–Cr-2, **d** ZnO–Cr-3

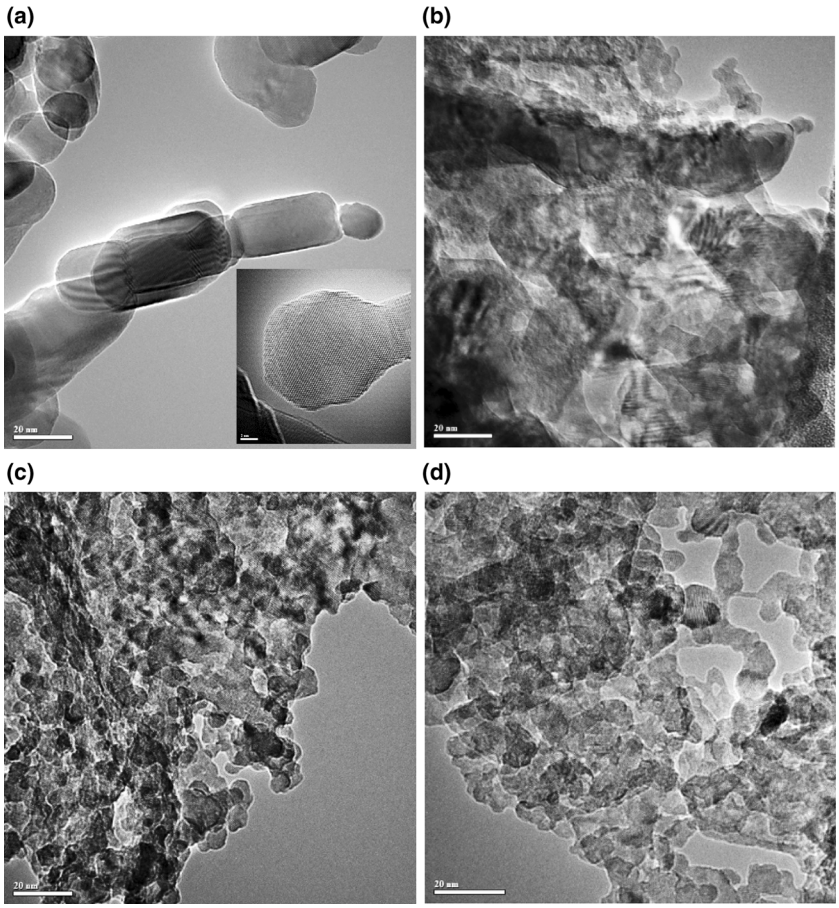

Fig. 3 TEM images of the samples: **a** ZnO, **b** ZnO–Cr-1, **c** ZnO–Cr-2, **d** ZnO–Cr-3

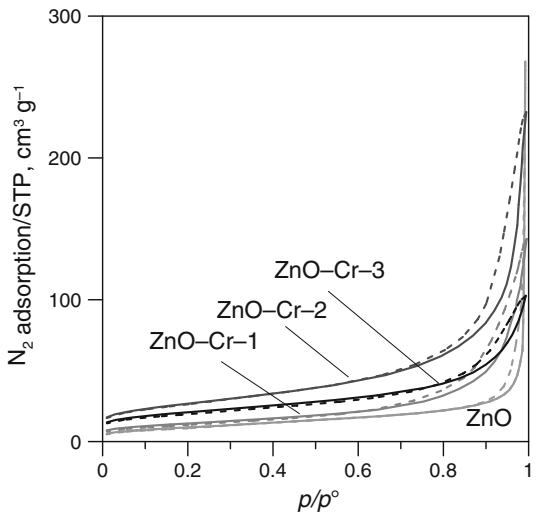

Fig. 4 Nitrogen adsorption–desorption isotherms of the samples

Accordingly, formation of ZnO–Cr–x high surface area materials can be connected with the presence of surface chromium phases, which may hinder fast growth and sintering of ZnO grains during precipitation and thermal treatment.

Redox properties

The temperature-programmed reduction curves of synthesized samples are presented in Fig. 5. No reduction peaks were detected below room temperature. The minor peak of hydrogen consumption for ZnO sample is observed at 250 °C. Small and wide peaks are also visible above 550 °C. These peaks can be attributed to the removal of surface oxygen by hydrogen. For chromium-modified zinc oxides, large irregular peaks are observed in the range of 200–350 °C. Consumption of hydrogen is connected with reduction of Cr^{6+} to Cr^{3+} [26, 27]. The temperature of main reduction maximum is gradually moved from 301 to 306 °C with an increase of chromium content. The shape of TPR peaks indicates the presence of oxide phases of different metal–oxygen bond strength. All samples contain small amounts of more difficult to reduce chromium phases, probably dispersed and strongly interacted with ZnO

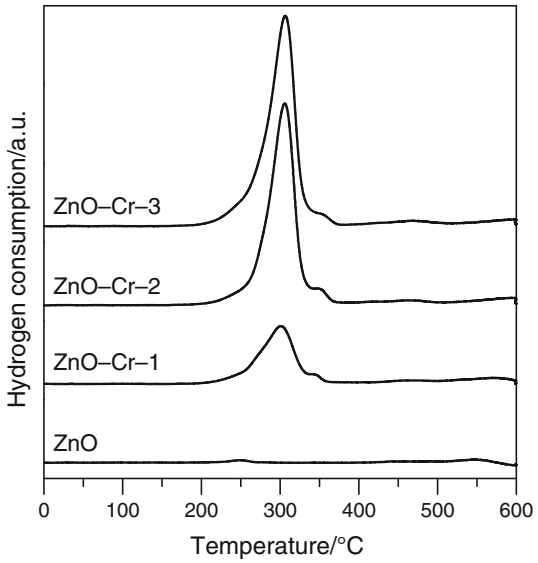

Fig. 5 Temperature-programmed reduction curves

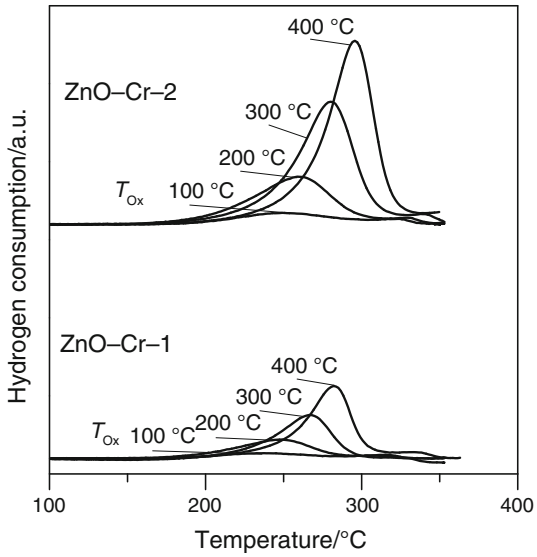

Fig. 6 Temperature-programmed reduction curves after oxidation of the samples at different temperatures ($T_{ox.}$)

species. TPR studies indicate that at least two types of adsorption sites can be present on the surface of chromium-modified zinc oxides, i.e. located on zinc oxide and assigned with chromium phases. The dual-site nature of the surface of oxides can be responsible for enhancement of some catalytic processes, e.g. related to simultaneous dehydrogenation/hydrogenation and reduction/oxidation processes.

Figure 6 shows temperature-programmed reduction curves, recorded after temperature-programmed oxidation of the obtained samples, carried out from −70 °C to the suitable temperature: 100, 200, 300 and 400 °C, respectively. Very small hydrogen consumption was observed for ZnO (not shown here). Thermal treatment of chromium-modified oxides in the oxidative atmosphere at low temperatures leads to the increase of the oxidation state of Cr^{3+} ions, probably located in the surface region of nanoparticles. The extent of the changes of oxidation state of Cr^{3+} ions rises with an increase of the treatment temperature and can be connected with participation of subsurface or inner sites in redox processes. Such effects are being accompanied by the changes of reducibility—an increase of the size of TPR peaks and shift of maxima towards higher temperatures. The TPR peaks become more pronounced and the maxima appear at higher temperatures as chromium content is increased. Studies indicate that the course of surface processes over chromium-modified zinc oxides may depend on the composition of oxides and the reaction conditions, including temperature and the presence of compounds with reductive or oxidative properties in the reaction mixture.

Methanol adsorption and desorption

Methanol adsorption and temperature-programmed desorption have been frequently used for characterization of the surface of catalysts [33–35]. It is well-accepted opinion that methanol can be adsorbed dissociatively on the surface of oxides with the formation of methoxy species (O–CH_3), and its further conversion depends on the properties of oxides and gas phase composition [35–37].

We have performed adsorption of methanol at 100 °C on the surface of pre-treated samples in the inert gas. The temperature-programmed desorption curves recorded by means of mass spectrometry are presented in Fig. 7. The concentration of selected major products, i.e. hydrogen ($m/e = 2$), carbon monoxide ($m/e = 28$) and carbon dioxide ($m/e = 44$), is displayed. The main products of methanol desorption from ZnO sample are carbon monoxide and hydrogen. Hydrogen is formed over ZnO sample above 150 °C. The shape of hydrogen desorption peak is relatively complex and results from the overlying of few desorption peaks with maxima at about 250, 300 and 340 °C. The maximum of the large carbon monoxide peak is observed at around 340 °C, while the maximum of very small carbon dioxide peak is visible at 300 °C. The decomposition of methanol towards hydrogen and carbon dioxide occurs much easier over chromium-modified zinc oxides. The first small peak of hydrogen starts nearly at 100 °C. Evolution of hydrogen occurs together with the formation of the small amounts of methanol, formaldehyde, water (not shown here) and larger amounts of carbon dioxide. The main peak of hydrogen is visible in the

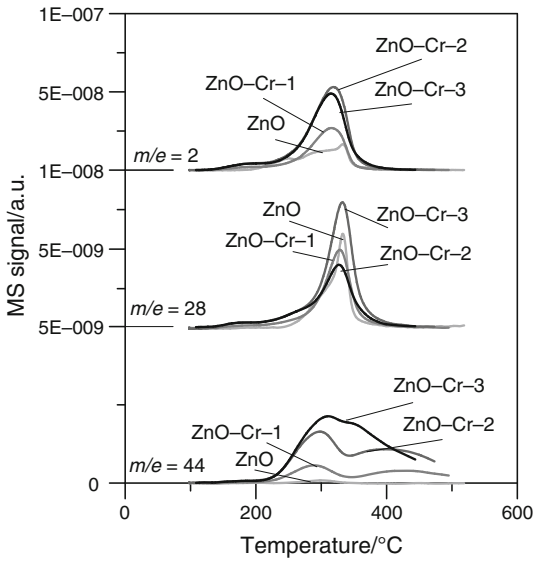

Fig. 7 MS—temperature-programmed desorption of methanol

temperature region of the evolution of carbon dioxide and then carbon monoxide.

DRIFTS spectra recorded during initial heating of calcined samples in the inert gas reveal the presence of hydroxyl groups bounded to different types of zinc and chromium sites (Fig. 8). In the case of ZnO, well-visible vibration bands of OH groups are observed at 3688, 3656, 3619, 3556, 3433 and 3379 cm^{-1}. Physically adsorbed water, hydrogen-bonded and weaker hydroxyl groups are

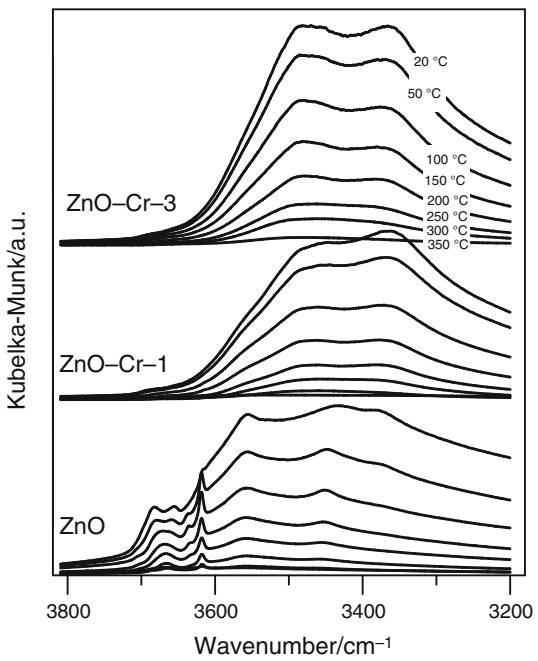

Fig. 8 DRIFTS spectra of the samples recorded at different temperatures during thermal treatment before adsorption of methanol

removed during thermal treatment at low temperatures. Very strong hydroxyl groups with vibration bands, located at higher wavenumbers, remain on the surface of pretreated samples at high temperatures, even at 350 °C. Different hydroxyl groups can be found on the surface of chromium-modified zinc oxides. The vibration bands in general are shifted to lower wavenumbers. The shift of stretching vibration bands towards lower wavenumbers can be ascribed to the O–H bond strength decrease and the same to the increase of Brønsted acidity of OH groups. This effect can be explained by the decrease of the electronic density between oxygen and hydrogen atoms, caused by cation electron-withdrawing phenomena. The frequency of the stretching vibration bands can be also influenced by the local environment of the sites and mutual interaction between hydroxyl groups, especially in porous material. The bands of hydroxyls located at high wavenumbers are almost invisible. ZnO nanoparticles in chromium-modified oxides are much smaller than in pure ZnO sample. The surface is more energetically heterogeneous due to point defects and the presence of chromium oxide species.

DRIFTS studies evidence that the way of methanol adsorption and surface reactions are related to the number and the nature of surface sites (Fig. 9). Methanol is adsorbed on the surface of ZnO at 100 °C mainly via formation of methoxy species [35–37]. The disappearance of vibration of hydroxyl groups located at higher wavenumbers during adsorption may indicate formation of strongly bounded species. The asymmetric $\nu_{as}(CH_3)$ and symmetric $\nu_s(CH_3)$ stretching vibrations after flushing of methanol at 100 °C are observed at 2931 and 2820 cm^{-1}, respectively. Slight peaks at 2888 and 2787 cm^{-1}, with weak shoulder at 2911 cm^{-1}, may indicate the presence of vibration bands of formate species ν(CH) adsorbed on the different ZnO planes [37–40]. In the fingerprint region (from 1700 to 650 cm^{-1}), the most pronounced band is located at 1071 cm^{-1}, which correspond to ν(CO) stretching vibrations in methoxy groups. Slight negative bands at 1504 and 1340 cm^{-1} can be ascribed to vibration bands of ν_{as}(OCO) and ν_s(OCO), related to the displacement of carbonate-like species.

The intensities of vibration bands of methoxy groups $\nu_{as}(CH_3)$ and $\nu_s(CH_3)$, as well as formate groups ν(CH), are slowly decreased during heating of the samples in the inert gas. New vibration bands of ν(CH), located at 2970 and 2870 cm^{-1}, are developed above 300 °C. Simultaneously, the intensity of the band at 1071 cm^{-1} is decreased and shifted to 1056 cm^{-1}, which is connected with the removal of methoxy groups of different thermal stability. Development of new bands at 1580, 1365 and 1380 cm^{-1}, assigned to asymmetric and symmetric stretching vibrations ν_{as}(OCO), ν_s(OCO), indicates gradual transformation of methoxy to formate species. The increase of intensity of

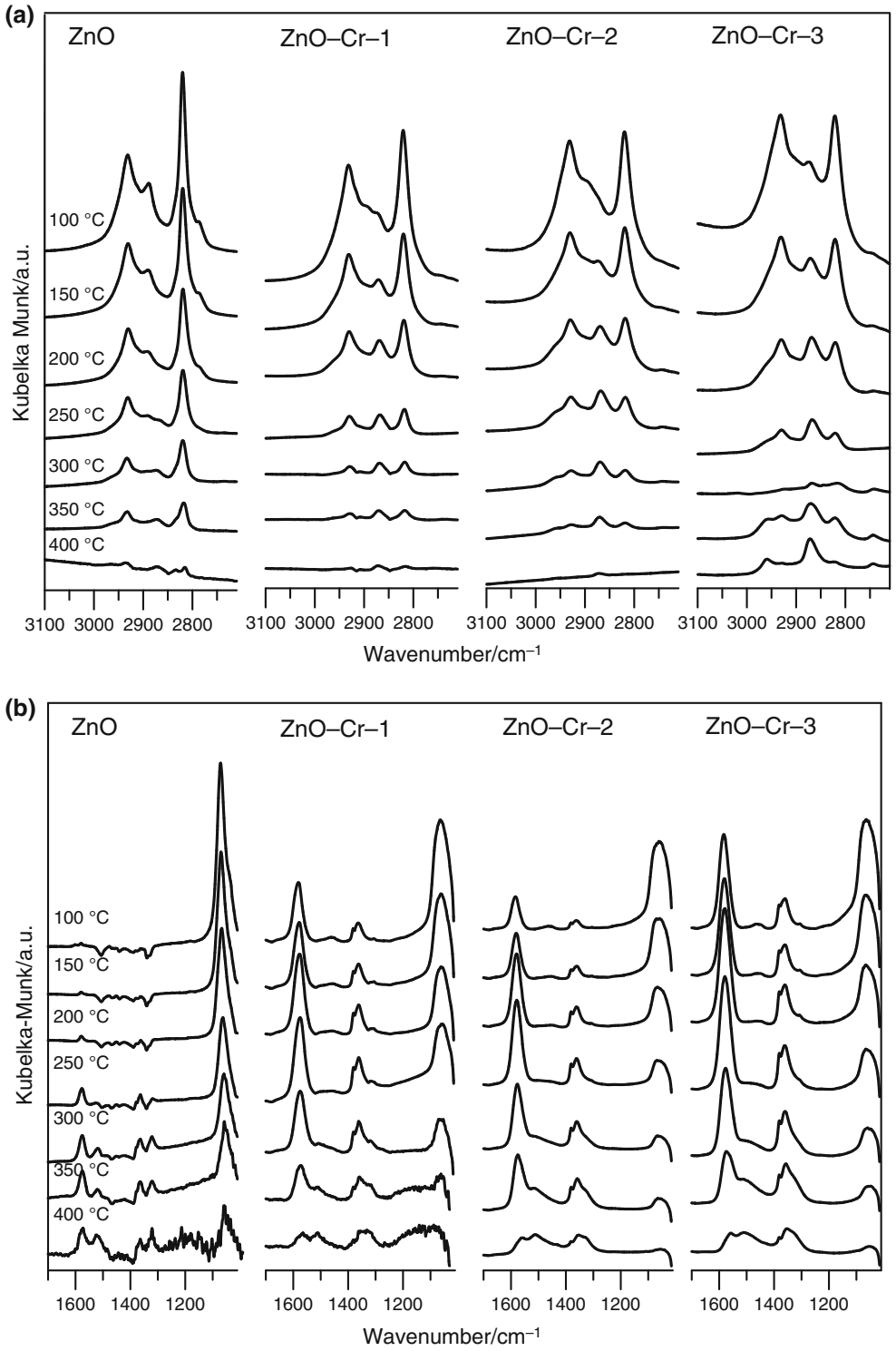

Fig. 9 DRIFTS spectra of the samples recorded at different temperatures during temperature-programmed desorption of methanol; **a** high wavenumber region, **b** fingerprint region

the bands at 1516 and 1321 cm^{-1} above 250 °C is due to the formation of carbonate-like species.

During adsorption of methanol over chromium-modified zinc oxides, similar phenomena connected with the decrease of intensity of hydroxyl bands located at higher wavenumbers are visible. The asymmetric $\nu_{as}(CH_3)$ and symmetric $\nu_s(CH_3)$ band vibrations of methoxy groups are observed at almost the same wavenumbers as for ZnO

sample. Strong band of formate species, observed for ZnO at 2888 cm^{-1} after flushing of methanol at 100 °C, appears as weak shoulder for modified oxides. Moreover, new vibration band of ν(CH) is visible at 2870 cm^{-1}. The intensity of this band strongly increases with an increase of desorption temperature. The pronounced changes of the way of methanol desorption are observed in the fingerprint region. Modification of zinc oxide with chromium facilitates formation of formate species at 100 °C. Strong stretching ν_{as}(OCO) and ν_s(OCO) vibration bands at 1580, 1361 and 1381 cm^{-1} are detected. The C–O stretching vibration bands ν_s(CO) of methoxy groups are located at around 1055 cm^{-1}. The intensity of methoxy groups decreases much easier than formates during temperature increase. The transformation of methoxy to formate and carbonate species is connected with dehydrogenation and oxidation surface processes. Such reactions may take place with participation of surface oxygen or hydroxyl groups. The enhancement of the transformation of the species over chromium-modified oxides can be connected with the presence of labile surface oxygen and the changes of the oxidation state of chromium ($Cr^{3+} \leftrightarrow Cr^{6+}$). Similar phenomena may improve catalytic activity and selectivity of copper or noble metal catalysts containing chromium-modified zinc oxide supports. Thus, formation of formates as intermediate species on the active metal sites, in such reactions as carbon dioxide hydrogenation or steam reforming of methanol, can be reinforced by the support.

Conclusions

Co-precipitation method was used for preparation of chromium-modified zinc oxides. The contents of chromium were varied from 3.33 to 17.1 mass%. We have shown that the presence of chromium influenced not only the size of particles, but also the structural properties of oxides and the chemical nature of the surface sites. The decrease of the mean crystallite size of ZnO was observed with an increase of chromium content. The specific surface area increased with the increase of chromium content up to 13 mass%. Chromium ions were partially incorporated to ZnO structure. Dispersed spinel ($ZnCr_2O_4$) and chromium zinc oxide ($ZnO{\cdot}CrO_3$) species were also detected. The possibility of the changes of the oxidation state of chromium in the reaction conditions was inferred. It was stated that methanol was adsorbed on the surface of obtained zinc oxide at 100 °C mainly via formation of methoxy species, and the main products of methanol desorption at higher temperatures were carbon monoxide and hydrogen. The presence of chromium in the prepared materials facilitated direct formation of formate species at low temperatures (100 °C) and their transformation to hydrogen and carbon dioxide at elevated temperatures.

Acknowledgements This work was carried out in part within the framework of European Union's Seventh Framework Programme for the Fuel Cells and Hydrogen Joint Technology Initiative under IRMFC Grant Agreement No. 325358. The research was carried out with the equipment purchased thanks to the financial support of the European Regional Development Fund in the framework of the Polish Innovation Economy Operational Program (Contract no. POIG.02.01.00-06-024/09 Center of Functional Nanomaterials).

References

1. Moezzi A, McDonagh AM, Cortie MB. Zinc oxide particles: synthesis, properties and applications. Chem Eng J. 2012;185–186:1–22.
2. Özgür Ü, Alivov YI, Liu C, Teke A, Reshchikov MA, Doğan S, Avrutin V, Cho SJ, Morkoç H. A comprehensive review of ZnO materials and devices. J Appl Phys. 2005;98:1–103.
3. Wang ZL. Zinc oxide nanostructures: growth, properties and applications. J Phys Condens Matter. 2004;16:R829–58.
4. Willander M, Nur O, Zhao QX, Yang LL, Lorenz M, Cao BQ, Pérez JZ, Czekalla C, Zimmermann G, Grundmann M, Bakin A, Behrends A, Al-Suleiman M, El-Shaer A, Che Mofor A, Postels B, Waag A, Boukos N, Travlos A, Kwack HS, Guinard J, Dang DLS. Zinc oxide nanorod based photonic devices: recent progress in growth, light emitting diodes and lasers. Nanotechnology. 2009;20:332001–3320040.
5. Rodnyi PA, Khodyuk IV. Optical and luminescence properties of zinc oxide (review). Opt Spectrosc. 2011;111:776–85.
6. Pillai SC, Kelly JM, Ramesh R, McCormack DE. Advances in the synthesis of ZnO nanomaterials for varistor devices. J Mater Chem C. 2013;1:3268–81.
7. Wei A, Pan L, Huang W. Recent progress in the ZnO nanostructure-based sensors. Mater Sci Eng B. 2001;176:1409–21.
8. Arya SK, Saha S, Ramirez-Vick JE, Gupta V, Bhansali S, Singhe SP. Recent advances in ZnO nanostructures and thin films for biosensor applications: review. Anal Chim Acta. 2012;737:1–21.
9. Liu C, Yun F, Morkoç H. Ferromagnetism of ZnO and GaN: a review. J Mater Sci Mater Electron. 2005;16:555–97.
10. Ahmad M, Ahmed E, Zhang Y, Khalida NR, Xu J, Ullah M, Hong Z. Preparation of highly efficient Al-doped ZnO photocatalyst by combustion synthesis. Curr Appl Phys. 2013;13:697–704.
11. Kołodziejczak-Radzimska A, Jesionowski T. Zinc oxide -from synthesis to application: a review. Materials. 2014;7:2833–81.
12. Lloyd L. Handbook of industrial catalysts. New York: Springer Science & Business Media; 2011.
13. Yang Y, Xie W. Soybean oil transesterification over zinc oxide modified with alkali earth metals. Fuel Process Technol. 2007;88:631–8.
14. Kumar BV, Naik HSB, Girija D, Kumar BV. ZnO nanoparticle as catalyst for efficient green one-pot synthesis of coumarins through Knoevenagel condensation. J Chem Sci. 2011;123:615–21.
15. Liu XM, Lu GQ, Yan YF, Beltramini J. Recent advances in catalysts for methanol synthesis via hydrogenation of CO and CO_2. Ind Eng Chem Res. 2003;42:6518–30.

16. Sá S, Silva H, Brandão L, Sousa JM, Mendes A. Catalysts for methanol steam reforming—a review. Appl Catal B Environ. 2010;99:43–57.
17. Maroto-Valer MM, Song C, Soong Y. Environmental challenges and greenhouse gas control for fossil fuel utilization in the 21st century. New York: Springer Science & Business Media; 2002.
18. Avgouropoulos G, Schlicker S, Schelhaas K-P, Papavasiliou J, Papadimitriou KD, Theodorakopoulou E, Gourdoupi N, Machocki A, Ioannides T, Kallitsis JK, Kolb G, Neophytides S. Performance evaluation of a proof-of-concept 70 W internal reforming methanol fuel cell system. J Power Sources. 2016;307:875–82.
19. Bergeret G, Gallezot P. In: Ertl G, Knozinger H, Weitkamp J, editors. Handbook of heterogeneous catalysis. Weinheim: VCH; 1997. p. 439.
20. Lowell S, Shields JE, Thomas MA, Thommes M. Characterization of porous solids and powders: surface area, pore size and density. Berlin: Kluwer Academic Publishers; 2004.
21. Liu Y, Yang Y, Guan Q, Liu H, Yang L, Zhang Y, Wang Y, Wei M, Liu X, Fei L, Cheng X. Intrinsic ferromagnetic properties in Cr-doped ZnO diluted magnetic semiconductors. J Solid State Chem. 2011;184:1273–8.
22. Shannon RD. Revised effective ionic radii and systematic studies of interatomic distances in halides and chalcogenides. Acta Cryst. 1976;A32:751–67.
23. Vaccari A. Clays and catalysis: a promising future. Appl Clay Sci. 1999;14:161–98.
24. Rives V, Ulibarri MA. Layered double hydroxides (LDH) intercalated with metal coordination compounds and oxometalates. Coord Chem Rev. 1999;181:61–120.
25. Kloprogge JTh, Hickey L, Frost RL. The effect of varying synthesis conditions on zinc chromium hydrotalcite: a spectroscopic study. Mater Chem Phys. 2005;89:99–109.
26. Fuda K, Suda K, Matsunaga T. Oxidation of Cr(III) to Cr(VI) species during the thermal decomposition process of Zn/Cr-layered double hydroxide carbonate. Chem Lett. 1993;22:1479–82.
27. Arco M, Rives V, Trujillano R, Malet P. Thermal behaviour of Zn–Cr layered double hydroxides with hydrotalcite-like structures containing carbonate or decavanadate. J Mater Chem. 1996;6:1419–28.
28. Naidu SR, Banerjee AK, Ganguli NC, Sen SP. Stoichiometric modifications of ZnO–Cr_2O_3 catalyst system in oxidizing and reducing atmospheres. J Res Inst Catal. 1973;21:172–86.
29. Errani E, Trifiro F, Vaccari A, Richter M, Del Pierro G. Structure and reactivity of Zn–Cr mixed oxides. Role of non-stoichiometry in the catalytic synthesis of methanol. Catal Lett. 1989;3:65–72.
30. Sing KSW. Reporting physisorption data for gas/solid systems. Pure Appl Chem. 1982;54:2201–18.
31. Maldonado A, Mallén-Hernández SA, Vega-Pérez J, de la L Olvera M, Tirado-Guerra S. Chromium doped zinc oxide thin films deposited by chemical spray used in photo-catalysis and gas sensing. Rev Mex Fis. 2009;55:90–4.
32. Tajizadegan H, Heidary A, Torabi O, Golabgir MH, Jamshidi A. Synthesis and characterization of $ZnCr_2O_4$ nanospinel prepared via homogeneous precipitation using urea hydrolysis. Int J Appl Ceram Technol. 2015;4:1–6.
33. Tatibouët JM. Methanol oxidation as a catalytic surface probe. Appl Catal A Gen. 1997;148:213–52.
34. Badlani M, Wachs IE. Methanol: a "smart" chemical probe molecule. Catal Lett. 2001;75:137–49.
35. Vargas MAL, Busca G, Costantino U, Marmottini F, Montanari T, Patrono P, Pinzari F, Ramis G. An IR study of methanol steam reforming over ex-hydrotalcite Cu–Zn–Al catalysts. J Mol Catal A Chem. 2007;266:188–97.
36. Strunk J, Kähler K, Xia X, Muhler M. The surface chemistry of ZnO nanoparticles applied as heterogeneous catalysts in methanol synthesis. Surf Sci. 2009;603:1776–83.
37. Kähler K, Holz MC, Rohe M, Strunk J, Muhler M. Probing the reactivity of ZnO and Au/ZnO nanoparticles by methanol adsorption: a TPD and DRIFTS study. Chem Phys Chem. 2010;11:2521–9.
38. Ueno A, Onishi T, Tamaru K. Reaction intermediates in methyl alcohol decomposition on ZnO. Trans Faraday Soc. 1971;67:3585–9.
39. Shido T, Iwasawa Y. Reactant-promoted reaction mechanism for water–gas shift reaction on ZnO, as the genesis of surface catalysis. J Catal. 1991;129:343–55.
40. Fujita S, Ito H, Takezawa N. Remarks on the assignments of temperature programmed desorption peaks for the surface species formed on Cu/ZnO and ZnO in the methanol synthesis from CO. Catal Lett. 1995;33:67–74.